

Nonlinear Operator Integration Factor Splitting for the Shallow Water Equations

Amik St-Cyr* and Stephen J. Thomas

*National Center for Atmospheric Research,
1850 Table Mesa Drive, Boulder, 80305 CO, USA*

Abstract

The purpose of this paper is to explore an alternative to the traditional interpolation based semi-Lagrangian time integrators employed in atmospheric models. A novel aspect of the present study is that operator splitting is applied to a purely hyperbolic problem rather than the incompressible Navier-Stokes equations. The underlying theory of operator integration factor splitting is reviewed and the equivalence with semi-Lagrangian schemes is established. A nonlinear variant of integration factor splitting is proposed where the advection operator is expressed in terms of the relative vorticity and kinetic energy. To preserve stability, a fourth order Runge-Kutta scheme is applied for sub-stepping. An analysis of splitting errors reveals that OIFS is compatible with the order conditions for linear multi-step methods. The new scheme is implemented in a spectral element shallow water model using an implicit second order backward differentiation formula for Coriolis and gravity wave terms. Numerical results for standard test problems demonstrate that much larger time steps are possible.

Key words: integration factor, multistep methods, high-order, spectral elements.

1 Introduction

The seminal work of Robert [24] led to a six-fold increase over the explicit time step for atmospheric general circulation models. To achieve such dramatic gains without recourse to a fully implicit integrator, a semi-Lagrangian treatment of advection was combined with a semi-implicit scheme for the stiff

* Corresponding author.

Email addresses: amik@ucar.edu (Amik St-Cyr), thomas@ucar.edu (Stephen J. Thomas).

terms responsible for gravity waves. Initially, semi-implicit semi-Lagrangian time-stepping was applied to hyperbolic problems, discretized using low-order finite-differences and finite elements [29]. However, the method was soon extended to global models based on the spectral transform [23]. The traditional semi-Lagrangian algorithm implemented in atmospheric models relies on backward trajectory integration and upstream interpolation. In effect, the numerical domain of dependence is shifted to an upstream grid cell and, for advective CFL numbers $C < 1$ with linear interpolation, is equivalent to upwind finite differencing. Upwind schemes are known to be diffusive and thus cubic interpolation has been generally adopted [28]. Indeed, McCalpin [19] has shown that high-degree polynomials are required in order to mitigate the inherent numerical dissipation and dispersion errors associated with semi-Lagrangian advection.

Bartello and Thomas [2] analyzed the cost-effectiveness of the backward semi-Lagrangian scheme in the context of geophysical flows. Their analysis was restricted to atmospheric models using low-order finite differences and either 2D or 3D Lagrangian interpolants. In the enstrophy cascade of homogeneous quasi-geostrophic turbulence, the authors concluded that high efficiency gains are possible over low-order Eulerian integrators. However, the gains are at best marginal in the case of a 3D Kolmogorov energy cascade. The cascade interpolation procedures of Purser and Leslie [21] and Nair et al. [20] reduce the computational complexity from $\mathcal{O}(N^d)$ to $\mathcal{O}(N)$ per grid point, where N is the degree of the interpolating polynomial in d space dimensions. The order of accuracy of these methods has not been formally established. Nevertheless, the time scale separation between Lagrangian and Eulerian frames is more restrictive for small-scale atmospheric dynamics when $E(k) \sim k^{-5/3}$ and the semi-Lagrangian scheme is only cost-effective at very high spatial resolutions.

The combination of the semi-Lagrangian approach together with a high-order spectral element space discretization, applied to the advection-diffusion equation, is described in Giraldo [12]. An important result of this study is that numerical dissipation and dispersion errors for the combined scheme are completely eliminated for polynomial order $N \geq 4$. More recently, Giraldo et al. [13] reported numerical results for a semi-Lagrangian semi-implicit shallow water model. Extension of the scheme to the hydrostatic primitive equations is discussed in Giraldo and Rosmond [14]. Motivated by the efficiency gains for advection-diffusion, Xiu and Karniadakis [33] applied a semi-Lagrangian spectral element (SESL) method to the incompressible Navier-Stokes equations. For laminar and transitional flows, they observed efficiency gains ranging from four to ten times over an Eulerian SE scheme. Xu et al. [35] simulated turbulent channel flow using a mixed spectral discretization. A ten-fold increase in the time-step was obtained, but only at the break-even point in computational efficiency due to the use of global interpolants. These results also confirm the error analysis of Falcone and Ferretti [9], who show that the error can actually

decrease as the time step increases.

In high-order methods, the computational cost of upstream interpolation for an N -th order discretization in d space dimensions is $\mathcal{O}(N^d)$ per degree of freedom. Given a spectral element discretization consisting of K elements of order N , there are KN^d grid points and the total interpolation cost is $\mathcal{O}(KN^{2d})$. By comparison, the cost of Eulerian operator evaluations scales as $\mathcal{O}(KN^{d+1})$. For example, advection of a scalar requires dKN^{d+1} operations [10]. A potentially lower cost alternative to interpolation is the operator integrating factor splitting (OIFS) method of Maday et al. [18] which relies on Eulerian sub-stepping of the advection equation. If the total number of sub-steps per time step is less than N^{d-1} , then OIFS should be more efficient. Boyd [3] observed that both semi-Lagrangian and OIFS algorithms are members of a broader class of integration factor methods.

There are several motivations for our evaluation of integration factor methods in the context of spectral elements applied to geophysical flows. The advective CFL number scales as $\mathcal{O}(N^{-2})$ and is more restrictive than a stability condition derived purely from dimensional analysis would indicate. Removing this restriction permits a significant increase in the time step. For example, allowing it to match the time scale of sub-grid scale physical parameterizations. In contrast with semi-Lagrangian advection, there are no dissipation or dispersion errors associated with upstream interpolation or trajectory integration and the scheme maintains the high-order accuracy of the underlying discrete spatial operators. For spectral elements, and finite elements in general, the discrete advection operator is skew-symmetric. The stability region of the integrator should contain part of the imaginary axis and thus a fourth-order explicit Runge-Kutta (RK-4) method is employed for sub-stepping.

For the incompressible Navier-Stokes equations, the zero divergence constraint must be maintained. In the linear OIFS scheme, this can be accomplished by interpolation and extrapolation of the velocity between time levels [6,10]. Fischer notes [10] that for a backward differentiation formula (BDF) with k time levels, the advection equation is integrated k times, resulting in a complexity scaling as $\mathcal{O}(k^2)$. However, the cost can be reduced to $\mathcal{O}(k)$ by exploiting linearity and superposition. For the shallow water equations, the divergence is non-zero and linearity is not a requirement. Wilhelm and Kleiser [31] demonstrate that the advective form and rotational form (vorticity and kinetic energy) of the advection operator are stable under the $\mathbb{P}_N - \mathbb{P}_{N-2}$ spectral element discretization. The rotational form is better suited to curvilinear coordinates in cubed-sphere geometry as Christoffel symbols are not present and the momentum equation can be written in flux form.

For the present study, a novel OIFS method has been implemented in the spectral element shallow water model developed by Thomas and Loft [30].

This nonlinear variant of the OIFS method is implemented using a fourth-order Runge-Kutta (RK-4) scheme for sub-stepping and a second-order BDF-2 method for the Coriolis and gravity wave terms. Numerical results are presented for test cases proposed by Williamson et al. [32]. Couzy [6] and Sherwin [27] observe that sub-stepping can induce an $\mathcal{O}(\Delta t)$ error for steady-state solutions of the incompressible Navier-Stokes equations. For a steady-state geostrophic shallow water flow, second order convergence is obtained, without evidence of splitting errors. In all cases, significantly larger time steps are possible when compared to both a semi-implicit Eulerian formulation and a linear variant of OIFS. The latter appears to break down due to extrapolation of the velocity. The recent results of Xiu et al. [34] for the incompressible Navier-Stokes equations appear to substantiate the findings of the present study. When combined with a conjugate gradient squared (CGS) algorithm, the model integration rate is accelerated by a factor of four over the explicit formulation.

2 Operator Integration Factor Splitting

Maday et al. [18] introduced a general splitting technique for systems of ordinary differential equations. To elucidate the operator integration factor splitting (OIFS) method, consider the initial value problem

$$\frac{du(t)}{dt} = S(u(t)) + F(u(t)), \quad t \in [t^0, T], \quad (1)$$

with initial condition $u(t = 0) = u_0$. $u \in \mathbb{R}^{\mathcal{N}}$, t is time and T is the final time of the integration. $S(u)$ and $F(u)$ are, in general, nonlinear functions. For example, $S(u)$ could represent the space-discretized advection operator and $F(u)$ the diffusion operator. Let us assume the existence of an integration factor $Q_S^{t^*}(t) \in \mathbb{R}^{\mathcal{N}} \times \mathbb{R}^{\mathcal{N}}$, such that

$$\frac{d}{dt} [Q_S^{t^*}(t) \cdot u(t)] = Q_S^{t^*}(t) \cdot F(u(t)), \quad (2)$$

The parameter t^* is an arbitrary fixed time $t^* \geq t$. Assuming that $Q_S^{t^*}(t^*) = I$, where I is the $\mathcal{N} \times \mathcal{N}$ identity matrix, it is straightforward to show that the integration factor satisfies the differential equation

$$\frac{d}{dt} [Q_S^{t^*}(t) \cdot u(t)] = -Q_S^{t^*}(t) \cdot S(u(t)). \quad (3)$$

If $S(u(t)) = A(t)u(t)$, where $A(t)$ is an $\mathcal{N} \times \mathcal{N}$ matrix, and $A(t_1)A(t_2) = A(t_2)A(t_1)$ for any times t_1 and t_2 , then

$$Q_S^{t^*}(t) = \exp \left[\int_t^{t^*} A(s) ds \right].$$

For matrices which do not commute, this formula does not apply. In particular, when A is time-independent, $Q_S^{t^*}(t) = e^{A(t^*-t)}$, and integration of (2) over the interval (t, t^*) yields the well-known variation of constants formula

$$u(t^*) = e^{A(t^*-t)}u(t) + \int_t^{t^*} e^{A(t^*-s)}F(u(s)) ds.$$

The latter is useful in the linear stability analysis of (1). Linearization is also important for determining the order conditions and splitting errors associated with time discretization schemes which approximate the application of the matrix exponential $e^{A(t^*-t)}$ or integration factor $Q_S^{t^*}(t)$ to a vector $u(t)$.

In order to simplify the notation and represent the application of the integration factor to a vector, an auxiliary vector $v^{(t^*,t)}(s) \in \mathbb{R}^{\mathcal{N}}$ is now introduced and the following result is established (see Deville et al. [7])

Theorem 1 *If $v^{(t^*,t)}(s)$ is the solution of*

$$\frac{d}{ds}v^{(t^*,t)}(s) = S(v^{(t^*,t)}(s)), \quad 0 \leq s \leq t^* - t \quad (4)$$

with initial condition $v^{(t^,t)}(0) = u(t)$, then $Q_S^{t^*}(t) \cdot u(t) = v^{(t^*,t)}(t^* - t)$.*

PROOF. Multiplying (4) by $Q_S^{t^*}(t+s)$, it follows that

$$Q_S^{t^*}(t+s) \frac{d}{ds}v^{(t^*,t)}(s) = Q_S^{t^*}(t+s)S(v^{(t^*,t)}(s)). \quad (5)$$

By making the change of variables $t \rightarrow t+s$ in (3), and substituting the initial condition $v^{(t^*,t)}(s) = u(s+t)$ of the shifted problem (4) on the interval $s \in (t, t^*)$, leads to

$$\frac{d}{ds} \left[Q_S^{t^*}(t+s) \right] \cdot v^{(t^*,t)}(s) = -Q_S^{t^*}(t+s)S(v^{(t^*,t)}(s)). \quad (6)$$

Addition of (5) and (6) yields the derivative

$$\frac{d}{ds} \left[(Q_S^{t^*})(t+s) \cdot v^{(t^*,t)}(s) \right] = 0.$$

The latter implies that $Q_S^{t^*}(t+s) \cdot v^{(t^*,t)}(s)$ is constant with respect to s . Setting $s = 0$ and exploiting the fact that $v^{(t^*,t)}(0) = u(t)$, the constant is seen to be

$Q_S^{t^*}(t) \cdot u(t)$. Thus, it follows that

$$Q_S^{t^*}(t+s) \cdot v^{(t^*,t)}(s) = Q_S^{t^*}(t) \cdot u(t).$$

Setting $t^* = t+s$ and applying the relation $Q_S^{t^*}(t^*) = I$ leads to the final result

$$Q_S^{t^*}(t) \cdot u(t) = v^{(t^*,t)}(t^* - t).$$

Now consider the situation where $S(u)$ represents the semi-discrete advection operator. The parameterized curve $X(x, t)$ represents the Lagrangian trajectory of a fluid particle with velocity $u(X(x, t), t)$, where the material or total derivative is

$$\frac{d}{dt}u(X(x, t), t) = \frac{\partial u(x, t)}{\partial t} - S(u(x, t)) \quad (7)$$

and $X(x, t)$ satisfies the ordinary differential equation

$$\frac{d}{dt}X(x, t) = u(X(x, t), t). \quad (8)$$

The next theorem establishes that OIFS is equivalent to a semi-Lagrangian method. However, rather than backward particle tracking followed by interpolation, the Eulerian advection equation is integrated forward in time.

Theorem 2 *If $X(x, t^{n-q})$ is the solution to the initial value problem*

$$\frac{d}{dt}X(x, t) = u(X(x, t), t), \quad t \in [t^{n-q}, t^n]$$

with $X(x, t^n) = x$ and $v^{(t^n, t^{n-q})}(s)$ is the solution of (4) with initial condition $v^{(t^n, t^{n-q})}(0) = u(x, t^{n-q})$ then

$$u(X(x, t^{n-q}), t^{n-q}) = v^{(t^n, t^{n-q})}(t^n - t^{n-q}).$$

PROOF. Integration of (7) on the interval $[t^{n-q}, t^n]$ results in

$$\int_{t^{n-q}}^{t^n} \frac{d}{ds}u(X(x, s), s)ds = \int_{t^{n-q}}^{t^n} \left\{ \frac{\partial u(x, s)}{\partial s} - S(u(x, s)) \right\} ds$$

$$u(X(x, t^n), t^n) - u(X(x, t^{n-q}), t^{n-q}) = u(x, t^n) - u(x, t^{n-q}) - \int_{t^{n-q}}^{t^n} S(u(x, s)) ds$$

where $u(X(x, t^n), t^n) = u(x, t^n)$ because $X(x, t^n) = x$. Thus,

$$u(X(x, t^{n-q}), t^{n-q}) = u(x, t^{n-q}) + \int_{t^{n-q}}^{t^n} S(u(x, s)) ds. \quad (9)$$

Then, for a fixed x the right hand side of (9) is the solution of the initial value problem

$$\frac{dv}{ds}(s) = S(v(s)), \quad t^{n-q} \leq s \leq t^n \quad (10)$$

with initial condition $v(0) = u(t^{n-q})$. The result trivially follows by recognizing that the problem (10) is the same as (4) on the shifted interval $s \in [t^{n-q}, t^n]$. Thus, the left hand side of (9) is equivalent to the solution of problem (4)

$$u(X(x, t^{n-q}), t^{n-q}) = v^{(t^n, t^{n-q})}(t^n - t^{n-q}).$$

To summarize, given a k level time discretization, the upstream value of $u(X(x, t^{n-q}), t^{n-q})$ is obtained by forward in time integration of the homogeneous advection equation

$$\frac{\partial \tilde{u}(x, t)}{\partial t} - S(\tilde{u}(x, t)) = 0, \quad t \in [t^{n-q}, t^n]$$

for time levels $n - q$, $q = 1, \dots, k$, with the initial conditions

$$\tilde{u}(x, t^{n-q}) = u(x, t^{n-q}).$$

It should be noted that the OIFS scheme is equivalent to semi-Lagrangian advection only when primitive variables are integrated using (4) and $S(u)$ is the advection operator.

3 The Shallow Water Equations

The shallow water equations have been used as a vehicle for testing promising numerical methods for many years by the atmospheric modeling community. They contain the essential wave propagation mechanisms admitted by the hydrostatic primitive equations employed in 3D models of the atmospheric general circulation (for a mathematical introduction to the subject consult [8]). Specifically, these represent a hyperbolic system of equations, admitting gravity and Rossby wave solutions. The latter are important for correctly capturing nonlinear atmospheric dynamics. The governing equations for the 2D inviscid flow of a free surface are the momentum and continuity equations

$$\frac{\partial \mathbf{v}}{\partial t} + (f + \zeta) \mathbf{k} \times \mathbf{v} + \frac{1}{2} \nabla (\mathbf{v} \cdot \mathbf{v}) + \nabla \Phi = 0, \quad (11)$$

$$\frac{\partial \Phi}{\partial t} + (\mathbf{v} \cdot \nabla) \Phi + (\Phi_0 + \Phi) \nabla \cdot \mathbf{v} = 0. \quad (12)$$

h is the height above sea level, \mathbf{v} is the horizontal velocity and $\Phi = gh$ the geopotential height. f is the Coriolis parameter and \mathbf{k} a unit vector in the

vertical direction. The geopotential height is decomposed into a perturbation about a constant base state, Φ_0 .

In the present study, the equations of motion are solved in a cubed-sphere geometry [26,25,22]. Let \mathbf{a}_1 and \mathbf{a}_2 be the covariant base vectors of the transformation between inscribed cube and spherical surface. $\mathbf{v} = \mathbf{v}(\lambda, \theta)$ is the horizontal velocity vector on the sphere. Covariant and contravariant components are given by $u_1 = \mathbf{v} \cdot \mathbf{a}_1$, $u_2 = \mathbf{v} \cdot \mathbf{a}_2$ and $\mathbf{v} = u^1 \mathbf{a}_1 + u^2 \mathbf{a}_2$. The metric tensor of the transformation is defined as $G_{ij} \equiv \mathbf{a}_i \cdot \mathbf{a}_j$. Covariant and contravariant vectors are related through the metric tensor, $u_i = G_{ij} u^j$, $u^i = G^{ij} u_j$, where $G^{ij} = (G_{ij})^{-1}$ and $G = \{\det(G_{ij})\}^{1/2}$. For equal angular coordinates, $-\pi/4 \leq x^1, x^2 \leq \pi/4$, the metric tensor is

$$G_{ij} = \frac{1}{r^4 \cos^2 x^1 \cos^2 x^2} \begin{bmatrix} 1 + \tan^2 x^1 & -\tan x^1 \tan x^2 \\ -\tan x^1 \tan x^2 & 1 + \tan^2 x^2 \end{bmatrix}$$

where $r^2 = 1 + \tan^2 x^1 + \tan^2 x^2$ and $G = 1/r^3 \cos^2 x^1 \cos^2 x^2$. The divergence and relative vorticity are then given by

$$\nabla \cdot \mathbf{v} = \frac{1}{G} \left[\frac{\partial}{\partial x^1} (G u^1) + \frac{\partial}{\partial x^2} (G u^2) \right], \quad \zeta = \frac{1}{G} \left[\frac{\partial u_2}{\partial x^1} - \frac{\partial u_1}{\partial x^2} \right]$$

The equations of motion are discretized in space using the $\mathbb{P}_N - \mathbb{P}_{N-2}$ spectral element method as in [30]. The cubed-sphere is partitioned into K elements Ω^k in which the dependent and independent variables are approximated by tensor-product polynomial expansions. The velocity is expanded in terms of the N -th degree Lagrangian interpolants h_i

$$\mathbf{v}_h^k(r_1, r_2) = \sum_{i=0}^N \sum_{j=0}^N \mathbf{v}_{ij} h_i(r_1) h_j(r_2)$$

and the geopotential is expanded using the $(N-2)$ -th degree interpolants \tilde{h}_i

$$\Phi_h^k(r_1, r_2) = \sum_{i=1}^{N-1} \sum_{j=1}^{N-1} \Phi_{ij} \tilde{h}_i(r_1) \tilde{h}_j(r_2)$$

A weak Galerkin formulation results from integration of the equations with respect to test functions and direct evaluation of inner products using Gauss-Legendre and Gauss-Lobatto-Legendre quadrature. C^0 continuity of the velocity is enforced at inter-element boundaries sharing Gauss-Lobatto-Legendre points and direct stiffness summation is then applied [7]. The advection operator in the momentum equation is then expressed in terms of the relative vorticity and kinetic energy, whereas the continuity equation relies on the velocity form. Wilhelm and Kleiser [31] have shown that the rotational form of the advection operator is stable for the $\mathbb{P}_N - \mathbb{P}_{N-2}$ spectral element discretization.

4 Time Discretization

In the context of the incompressible Navier-Stokes equations, to integrate the time-split system (4) for the momentum equation, the OIFS algorithm described by Fischer [10] and Sherwin [27] employs an approximate linear advection equation

$$\frac{\partial \tilde{\mathbf{v}}}{\partial s} + \mathbf{v} \cdot \nabla \tilde{\mathbf{v}} = 0, \quad s \in [t^{n-q}, t^n], \quad (13)$$

with initial condition $\tilde{\mathbf{v}}(\mathbf{x}, t^{n-q}) = \mathbf{v}(\mathbf{x}, t^{n-q})$. To preserve a divergence free velocity field, \mathbf{v} is computed on $[t^{n-q}, t^{n-1}]$ by interpolation of known fields $\mathbf{v}^{n-k}, \mathbf{v}^{n-k+1}, \dots, \mathbf{v}^{n-1}$ and values of \mathbf{v} on the interval $(t^{n-1}, t^n]$ are extrapolated. Direct stiffness summation is applied every time step. Fischer [10], observes that the computational cost of an OIFS implementation can be reduced to $\mathcal{O}(k)$ by recognizing that (13) is linear and then exploiting superposition. In the case of the nonlinear shallow water equations, the flow field is divergent. Furthermore, our numerical experiments indicate that extrapolation leads directly to instabilities, thus limiting the maximum allowable time step for the system of equations (2).

The Courant-Friedrichs-Levy (CFL) number is $C = \max |\lambda| \Delta t$ and for spectral elements, $\max |\lambda| = \sigma |\mathbf{v}| / \Delta x_{\min}$ where σ ranges between 1.52 and 1.16 as the polynomial order N increases. Δx_{\min} scales as $\mathcal{O}(N^{-2})$ due to the clustering of Gauss-Lobatto-Legendre points at element interfaces. In general, the eigenvalue spectrum of the discrete advection operator includes some part of the imaginary axis. For example, in the case of spectral elements, the linear advection operator is skew-symmetric with purely imaginary eigenvalues. Therefore, any time integration scheme for sub-stepping (13) should have a stability region that includes a portion of the imaginary axis. Third and fourth order explicit Runge-Kutta methods are thus appropriate for sub-stepping. The CFL number for the third order RK-3 scheme is $C = 1.73$, representing the intersection of the stability region with the imaginary axis. Three function evaluations are required in RK-3, implying an efficiency factor of $C/3 = 0.58$, whereas RK-4 requires four function evaluations and $C = 2.82$, yielding an efficiency factor of 0.70 (see Durran [8]). For this reason, an RK-4 scheme is adopted to integrate (13). Long integrations could result in significant phase and dissipation errors as observed by Hu et al. [15].

To exploit the potential of OIFS for systems of time-dependent partial differential equations, it is our contention that the fully nonlinear form of the initial value problem (4) is more appropriate for integration factor splitting. In the case of the shallow water equations, therefore, sub-stepping is applied to the

equations

$$\frac{\partial \tilde{\mathbf{v}}}{\partial s} + \tilde{\zeta} \mathbf{k} \times \tilde{\mathbf{v}} + \frac{1}{2} \nabla (\tilde{\mathbf{v}} \cdot \tilde{\mathbf{v}}) = 0, \quad (14)$$

$$\frac{\partial \tilde{\Phi}}{\partial s} + (\tilde{\mathbf{v}} \cdot \nabla) \tilde{\Phi} + \tilde{\Phi} \nabla \cdot \tilde{\mathbf{v}} = 0. \quad (15)$$

with initial conditions $\tilde{\mathbf{v}}(\mathbf{x}, t^{n-q}) = \mathbf{v}(\mathbf{x}, t^{n-q})$, $\tilde{\Phi}(\mathbf{x}, t^{n-q}) = \Phi(\mathbf{x}, t^{n-q})$. Note that (15) is in fact the conservative form of the continuity equation

$$\frac{\partial \tilde{\Phi}}{\partial s} + \nabla \cdot (\tilde{\Phi} \tilde{\mathbf{v}}) = 0. \quad (16)$$

According to equation (2), the integration factor $Q_S^{t^*}(t)$ is applied to the remaining de-coupled system of equations containing the Coriolis and linear gravity wave terms

$$\frac{d}{dt} Q_S^{t^*}(t) \begin{bmatrix} \mathbf{v} \\ \Phi \end{bmatrix} = -Q_S^{t^*}(t) \begin{bmatrix} f \mathbf{k} \times \mathbf{v} + \nabla \Phi \\ \Phi_0 \nabla \cdot \mathbf{v} \end{bmatrix}. \quad (17)$$

An accurate representation of fast-moving gravity waves is not required for large scale atmospheric dynamics and the corresponding terms can be treated implicitly. For an implicit second order BDF-2 scheme, sub-stepping of the right-hand-side terms is not required because $Q_S^{t^n}(t^n) = I$. The resulting time discretization of (17) is given by

$$\frac{3\mathbf{v}^n - 4\tilde{\mathbf{v}}^{n-1} + \tilde{\mathbf{v}}^{n-2}}{2\Delta t} = -\mathbf{M}f\mathbf{v}^n - \nabla \Phi^n \quad (18)$$

$$\frac{3\Phi^n - 4\tilde{\Phi}^{n-1} + \tilde{\Phi}^{n-2}}{2\Delta t} = -\Phi_0 \nabla \cdot \mathbf{v}^n \quad (19)$$

where the value of the fields $\tilde{\mathbf{v}}$ and $\tilde{\Phi}$ at time levels $n-1$ and $n-2$ are computed by sub-stepping (14) and (15) on the intervals $[t^{n-1}, t^n]$ and $[t^{n-2}, t^n]$. It is then straightforward to de-couple the above system of equations, yielding

$$\mathbf{v}^n + \frac{2}{3} \Delta t \mathbf{N} \nabla \Phi^n = \frac{4}{3} \mathbf{N} \tilde{\mathbf{v}}^{n-1} - \frac{1}{3} \mathbf{N} \tilde{\mathbf{v}}^{n-2} \quad (20)$$

$$\Phi^n + \frac{2}{3} \Delta t \Phi_0 \nabla \cdot \mathbf{v}^n = \frac{4}{3} \tilde{\Phi}^{n-1} - \frac{1}{3} \tilde{\Phi}^{n-2} \quad (21)$$

where

$$\mathbf{N} = \left(I + \frac{2}{3} \Delta t f \mathbf{M} \right)^{-1}, \quad \mathbf{M} = \begin{bmatrix} 0 & -1 \\ 1 & 0 \end{bmatrix} \quad (22)$$

An implicit equation for Φ^n is obtained after spectral element discretization and application of block Gaussian elimination, resulting in a reduced Schur complement system. The coefficient matrix of this linear system of equations

is non-symmetric due to the implicit treatment of the Coriolis terms and is solved using an iterative conjugate-gradient squared (CGS) algorithm. Once Φ^n has been computed, \mathbf{v}^n is obtained by back-substitution.

5 Splitting Error Analysis

The general class of linear multistep methods for ordinary differential equations includes the second order backward differentiation formula employed in the present study. An analysis of the stability and accuracy of these methods can be found in the texts [16,4]. The notation adopted here closely follows [16]. Consider the linear version of the initial value problem (1)

$$\frac{du(t)}{dt} = Su(t) + Fu(t). \quad (23)$$

If the initial condition is specified at t^n , then the solution at t^{n+k} is exactly

$$u(t^{n+k}) = e^{k\Delta t(S+F)}u(t^n). \quad (24)$$

Solving first for S and then F , the solution is given by

$$u(t^{n+k}) = e^{k\Delta tF}e^{k\Delta tS}u(t^n). \quad (25)$$

Hence the splitting error is the difference between (24) and (25) and the order of accuracy depends on the commutativity of the matrices S and F . When these matrices do not commute, the splitting is only first order accurate.

A k -step linear multistep method for integrating (2) is given by

$$\sum_{j=0}^k \alpha_j Q_S^{t^{n+k}}(t^{n+j})u^{n+j} = \Delta t \sum_{j=0}^k \beta_j Q_S^{t^{n+k}}(t^{n+j})Fu^{n+j}.$$

The action of the integrating factor in the linear autonomous case is

$$Q_S^{t^{n+k}}(t^{n+j})u^{n+j} = e^{\Delta t(k-j)S}u^{n+j}.$$

Collect the terms at time level $n+k$ on the left-hand side, and substitute for $u^{n+j} = e^{(j-l)\Delta t(S+F)}u^{n+l}$

$$(I - \Delta t \bar{\beta}_k F)u^{n+k} = \sum_{j=0}^{k-1} e^{(k-j)\Delta tS} (\Delta t \bar{\beta}_j F - \bar{\alpha}_j I) e^{(j-l)\Delta t(S+F)} u^{n+l}.$$

where $(\bar{\alpha}_j, \bar{\beta}_j) = (\alpha_j, \beta_j)/\alpha_k$. Expand the inverse of the matrix appearing on the left-hand side

$$(I - \Delta t \bar{\beta}_k F)^{-1} = \sum_{m=0}^{\infty} (\Delta t \bar{\beta}_k F)^m$$

and it follows that

$$u^{n+k} = \sum_{m=0}^{\infty} \sum_{j=0}^{k-1} (\Delta t \bar{\beta}_k F)^m e^{(k-j)\Delta t S} (\Delta t \bar{\beta}_j F - \bar{\alpha}_j I) e^{(j-l)\Delta t(S+F)} u^{n+l}. \quad (26)$$

If the numerical method to compute $Q_S^{t^{n+k}} u^{n+j}$ is order p , then the Taylor series of the matrix exponential $e^{(k-j)\Delta t S}$ is exact up to the $p + 1$ -st term. Thus, for a third second accurate scheme, the exponentials can be expanded up to third order

$$e^{(k-j)\Delta t S} = I + (k-j)\Delta t S + \frac{1}{2}(k-j)^2 \Delta t^2 S^2$$

Substitute the above equation into (26) and, for $k = 2$, retain all terms up to $\mathcal{O}(\Delta t^2)$. Subtract the resulting expression from the Taylor series expansion of the exact solution $u(t^{n+k}) = e^{(k-l)\Delta t(S+F)} u(t^{n+l})$. Then the following conditions must be satisfied.

$$-\bar{\alpha}_0 - \bar{\alpha}_1 = 1 \quad (27)$$

$$\bar{\beta}_0 + \bar{\beta}_1 + \bar{\beta}_2 - \bar{\alpha}_1 = 2 \quad (28)$$

$$2\bar{\beta}_2 - \frac{\bar{\alpha}_1}{2} + \bar{\beta}_1 = 2 \quad (29)$$

$$\bar{\beta}_1 + 2\bar{\beta}_0 - \frac{3\bar{\alpha}_1}{2} = 2 \quad (30)$$

$$\bar{\beta}_2^2 - (\bar{\beta}_1 + \bar{\beta}_0 + \bar{\alpha}_1)\bar{\beta}_2 - \frac{\bar{\alpha}_1}{2} + \bar{\beta}_1 - 2 = 0 \quad (31)$$

A k -step method is order p if the coefficients satisfy the order conditions

$$\sum_{j=0}^k \alpha_j = 0, \quad \sum_{j=0}^k \alpha_j j^i = i \sum_{j=0}^k \beta_j j^{i-1}.$$

Equations (27), (28) and (29) are none other than these order conditions and are automatically satisfied. Combining the order conditions (29) and (28) results in (30). Finally, substituting (29) into the quadratic (31) leads to

$$\bar{\beta}_2(\bar{\beta}_2 + \bar{\beta}_1 + \bar{\beta}_0 - \bar{\alpha}_1 - 2) = 0$$

which is always satisfied due to the order condition (28).

The OIFS method is therefore second order accurate in the linear case, even when the matrices do not commute. To the best of our knowledge, this is the first formal proof of second order accuracy. Numerical experiments in the next section demonstrate that second order accuracy is achieved for the nonlinear shallow water equations.

6 Numerical Results

A standard test set for evaluating numerical approximations to the shallow water equations in spherical geometry was proposed by Williamson et al. [32]. To facilitate the comparison of different numerical methods, the authors provide definitions of l_1 , l_2 and l_∞ relative error metrics and flow invariants. Test case 2 is a stationary zonal geostrophic flow, representing a balance between the Coriolis and geopotential gradient forces in the momentum equation. The velocity field on the sphere is specified initially (and for all time) as

$$\begin{aligned} u &= u_0 (\cos \theta \cos \alpha + \cos \lambda \sin \theta \sin \alpha) \\ v &= -u_0 \sin \lambda \sin \alpha . \end{aligned}$$

where (λ, θ) are spherical longitude and latitude coordinates. α is the angle between the axis of solid body rotation and the polar axis. The analytic geopotential field $\Phi = gh$ is specified as

$$\Phi = \Phi_0 - \left(a\Omega u_0 + \frac{u_0^2}{2} \right) \times (-\cos \lambda \cos \theta \sin \alpha + \sin \theta \cos \alpha)^2 .$$

a is the radius of the earth and Ω is the rotation rate. Parameter values are specified to be $u_0 = 2\pi a/(12 \text{ days})$ and $\Phi_0 = 2.94 \times 10^4 \text{ m}^2/\text{s}^2$. The Coriolis parameter associated with this solution is

$$f = 2\Omega (-\cos \lambda \cos \theta \sin \alpha + \sin \theta \cos \alpha) .$$

The spectral element shallow water model was integrated for five days using both the extrapolated and nonlinear OIFS schemes. The total number of elements was 96, with 14×14 Gauss-Legendre points per element. A Fischer-Mullen [11] filter, was applied after every RK-4 time step and at the end of the BDF-2 time step. The BDF-2 time step was $\Delta t = 120 \text{ sec}$, corresponding to twice the explicit CFL number and the filter viscosity factor was $\mu = 0.01$. Figure 1 is a plot of the geopotential height l_2 error for both schemes and they exhibit comparable errors. The l_2 error for the nonlinear scheme oscillates slightly but is well below the time truncation error.

A second set of five day integrations was performed in order to evaluate the stability of the two methods and to confirm that the BDF-2/RK-4 time-stepping scheme is second order. 150 spectral elements and 8×8 Gauss points per element were employed. The filter viscosity factor was set at $\mu = 0.001$ for these simulations. Here, the time step is varied by two orders of magnitude. Figure 2 is a log-log plot of the geopotential height l_2 error versus the time step (scaled with respect to the explicit CFL number) for a five day integration. The plot clearly indicates that the extrapolated OIFS scheme becomes unstable at 15 times the explicit CFL number, whereas the nonlinear OIFS scheme remains

stable out to a time step that is 53 times larger than the explicit time step. The slope of the error curve in Figure 2 indicates that the nonlinear BDF-2/RK-4 scheme is indeed second order accurate.

Test case 5 is a zonal flow impinging on a mountain. The mean equivalent depth of the atmosphere is set to $h_0 = 5960$ meters. The mountain height is given by $h_s = h_{s_0}(1 - r/R)$, where $h_{s_0} = 2000$ m, $R = \pi/9$, and $r^2 = \min[R^2, (\lambda - \lambda_c)^2 + (\theta - \theta_c)^2]$. The center of the mountain is located at $\lambda_c = 3\pi/2$ and $\theta_c = \pi/6$ in spherical coordinates. An exact solution is not known and relative error metrics are computed by comparing against a T213 spectral transform reference solution. Numerical results are reported for the BDF-2/RK-4 integrator based on the nonlinear OIFS scheme and the Crank-Nicholson/leap-frog (CNLF) semi-implicit scheme described in Thomas and Loft [30]. A total of 150 spectral elements containing 8×8 Gauss-Legendre points are employed. The Fischer-Mullen filter was applied again with viscosity factor $\mu = 0.01$. The geopotential height l_2 error is plotted in Figure 3 for a fifteen day integration. The stable explicit time step is $\Delta t = 90$ sec and the CNLF scheme increases this by a factor of four. The BDF-2/RK-4 scheme further increases the explicit time step by a factor of 160. The l_2 errors for both models are comparable at $\Delta t = 360$ sec. When the BDF-2/RK-4 integrates at twenty times the effective CFL limit of the CNLF scheme, the l_2 error is slightly less than two times larger. For $\Delta t = 14400$ sec (not shown), the l_2 error at 15 days is approximately seven times larger.

In the presence of stationary forcing due to mountains, the traditional CNLF semi-implicit semi-Lagrangian scheme exhibits a resonance phenomena. Off-centering the Crank-Nicholson scheme introduces dissipation and thus mitigates the resonance problem. However, the resulting scheme is only first order accurate in time. Côté et al. [5] analyzed the linear stability of a family of second order integrators including BDF-2, which the authors refer to as ‘backward implicit’. They illustrate how the numerical dissipation of the BDF-2 scheme increases with the time step. The relative mass loss for the CNLF and BDF-2/RK-4 schemes is plotted in Figure 4 for different time steps and is observed to be of the same order of magnitude. Figure 5 contains polar cylindrical plots of the geopotential height field after 15 days of integration using $\Delta t = 480$ sec and $\Delta t = 7200$ sec. The effect of increased dissipation can be observed where the two separate 5900 meter isolines in the top panel have merged into a single isoline in the bottom panel.

The initial condition for test case 6 is a wavenumber four Rossby-Haurwitz wave. These waves are an ideal test because they represent exact analytic solutions to the nonlinear non-divergent barotropic vorticity equation. Rossby-Haurwitz waves are not closed-form solutions of the barotropic shallow water equations. A $1734 \times 8 \times 8$ spectral element grid was chosen in order to compare against the simulation results reported by Thomas and Loft in [30]. The

Fischer-Mullen filter viscosity factor was again set to $\mu = 0.01$. Because the advecting wind speed exceeds 50 ms^{-1} , the efficiency gains possible with the BDF-2/RK-4 scheme are somewhat diminished. BDF-2/RK-4 is only capable of taking time steps which are four times larger than the CNLF scheme, or 32 times larger than the explicit CFL. The geopotential height l_2 errors for a 14 day integration are plotted in Figure 6. Figure 7 contains polar cylindrical plots of the geopotential height field after 14 days using $\Delta t = 120 \text{ sec}$ and $\Delta t = 360 \text{ sec}$. The increased dissipation of the BDF-2 scheme is evident at the larger time step.

Although the implementation of the BDF-2/RK-4 scheme is still at an experimental stage, it leads to a significant increase in the model integration rate. Figure 8 is a plot of the ratio of CNLF and BDF-2/RK-4 execution times for test case 5. The efficiency gain of BDF-2/RK-4 over the CNLF scheme is close to a factor of two. Thomas and Loft [30] observed that the CNLF scheme integrated twice as fast as an explicit spectral element shallow water model. Therefore, the total increase in the model integration rate, when compared to the explicit model, is a factor of four. The plateau in the efficiency curve is due to a growing number of CGS iterations as the time step increases. Thus, computational cost of the time step is dominated by the Krylov solver. For the Rossby-Haurwitz test case 6, the computational efficiency is currently equivalent to the CNLF scheme (i.e. the efficiency ratio is close to 1). Further optimization of the nonsymmetric Krylov solver is possible. For example, a bi-conjugate gradient (BCG) algorithm [1] could lead to further improvements in computational efficiency.

7 Conclusions

A nonlinear variant of the OIFS method has been developed and applied to a hyperbolic system of partial differential equations. The advocated approach offers several advantages but some open questions remain. For example, it is not obvious how to group terms together at the same time level for sub-stepping as in the traditional semi-Lagrangian method. Unlike primitive variables, nonlinear forcing results in cross terms. Without the superposition principle, the optimizations proposed by Fischer [10] are not applicable. However, sub-stepping a nonlinear system permits much larger time steps. For extrapolated velocity fields, the time step is severely constrained in the case of the shallow water equations. The time step is also restricted in the case of the incompressible Navier-Stokes equations, as observed by Xiu et al. [34]

The splitting error analysis presented in this paper is restricted to linear non-commutative operators. However, our numerical results indicate that the BDF-2/RK-4 time stepping scheme is second order accurate. It should be noted that

for OIFS, steady state solutions are problematic. The difficulty stems from the fact that a fixed point solution of the full system might not be a steady state solution when operators are split (see locally one dimensional methods in Hundsdorfer and Verwer [16]). However, in the linear non-commutative case, a simple analysis shows that the fixed points of the global operator are the same as the two split ones. This result is confirmed by Krogstag [17] where the link between OIFS and exponential time differencing methods is made and numerically by Couzy [6] and, independently, by Sherwin [27]. To the best of our knowledge, a proof is not available in the nonlinear case.

The goal of our work is to develop a time-stepping scheme that is compatible with adaptive mesh refinement (AMR) for the 3D hydrostatic primitive equations employed in atmospheric general circulation models. Because these equations are ill-posed for any specification of point-wise boundary conditions, local time-stepping in refined regions should be avoided. One possible strategy is to apply the nonlinear OIFS scheme and sub-step based on the most restrictive CFL number. The observed computational efficiency is dominated by the cost of the Krylov iterative solver and thus additional sub-stepping does not add a significant computational overhead.

Acknowledgements The authors would like to thank Ram Nair for reviewing the manuscript and providing many helpful suggestions. We would also like to thank Paul Fischer for insightful discussions and sending a preprint of his unpublished manuscript. This work was partially supported by NSF Collaborations in Mathematics and Geosciences (CMG) grant 0222282 and the DOE climate change prediction program (CCPP).

References

- [1] BARRETT, R., BERRY, M., CHAN, T. F., DEMMEL, J., DONATO, J., DONGARRA, J., EIJKHOUT, V., POZO, R., ROMINE, C., AND DER VORST, H. V. *Templates for the Solution of Linear Systems: Building Blocks for Iterative Methods*. SIAM, Philadelphia, PA, 1994.
- [2] BARTELLO, P., AND THOMAS, S. J. The cost-effectiveness of semi-Lagrangian advection. *Mon. Wea. Rev.* 124, 12 (1996), 2883–2897.
- [3] BOYD, J. P. *Chebyshev and Fourier Spectral Methods*. Dover publications, 2001.
- [4] BUTCHER, J. C. *Numerical Methods for Ordinary Differential Equations*. John Wiley and Sons, 2003.
- [5] CÔTÉ, J., GRAVEL, S., AND STANFORTH, A. A generalized family of schemes that eliminates the spurious resonant response of semi-Lagrangian schemes to orographic forcing. *Mon. Wea. Rev.*, 123 (1995), 3605–3613. Notes and correspondence.
- [6] COUZY, W. *Spectral element solution discretization of the unsteady Navier-Stokes equations and its iterative solution on parallel computers*. PhD thesis, École polytechnique de Lausanne, EPFL, 1995.
- [7] DEVILLE, M. O., FISCHER, P. F., AND MUND, E. H. *High-Order Methods for Incompressible Fluid Flow*. Cambridge monographs on applied and computational mathematics. Cambridge University Press, 2002.
- [8] DURRAN, D. R. *Numerical Methods for Wave Equations in Geophysical Fluid Dynamics*, vol. 32 of *Texts in Applied Mathematics*. Springer-Verlag, 1999.
- [9] FALCONE, M., AND FERRETTI, R. Convergence analysis for a class of high-order semi-Lagrangian advection schemes. *SIAM J. Numer. Anal.* 35, 3 (1998), 909–940.
- [10] FISCHER, P. F. Implementation considerations for the OIFS/characteristics approach to convection problems. Manuscript, 2003.
- [11] FISCHER, P. F., AND MULLEN, J. S. Filter-based stabilization of spectral element methods. *C. R. Acad. Sci. Sér. I - Anal. Numér.* 332 (2001), 265–270.
- [12] GIRALDO, F. X. The Lagrange-Galerkin spectral element method on unstructured quadrilateral grids. *J. Comput. Phys.* 147 (1998), 114–146.
- [13] GIRALDO, F. X., PEROT, J. B., AND FISCHER, P. F. A spectral element semi-Lagrangian (SESL) method for the spherical shallow water equations. *J. Comput. Phys.* 190 (2003), 623–650.
- [14] GIRALDO, F. X., AND ROSMOND, T. E. R. A scalable spectral element Eulerian atmospheric model (SEE-AM) for NWP: Dynamical core. *Mon. Wea. Rev.* 132 (2004), 133–153.

- [15] HU, F. Q., HUSSAINI, M. Y., AND MANTHEY, J. L. Low-dissipation and low-dispersion Runge-Kutta schemes for computational acoustics. *J. Comput. Phys.* 124 (1996), 177–191.
- [16] HUNSDORFER, W., AND VERWER, J. G. *Numerical Solution of Time-Dependent Advection-Diffusion-Reaction Equations*. Series in Computational Mathematics. Springer-Verlag, 2003.
- [17] KROGSTAD, S. Generalized integrating factor methods for stiff PDEs. *preprint submitted to Elsevier science* (2003).
- [18] MADAY, Y., PATERA, A. T., AND RØNQUIST, E. M. An operator-integration-factor splitting method for time-dependent problems: Application to incompressible fluid flow. *J. Sci. Comput.* 5, 4 (1990), 263–292.
- [19] MCCALPIN, J. D. A quantitative analysis of the dissipation inherent in semi-Lagrangian advection. *Mon. Wea. Rev.* 116 (1998), 2330–2336.
- [20] NAIR, R. D., CÔTÉ, J., AND STANFORTH, A. Monotonic cascade interpolation for semi-Lagrangian advection. *Quart. J. Roy. Met. Soc.* 125 (1999), 197–212.
- [21] PURSER, R. J., AND LESLIE, L. M. An efficient interpolation procedure for high-order three-dimensional semi-Lagrangian models. *Mon. Wea. Rev.* 119 (1991), 2492–2498.
- [22] RANČIĆ, M. R., PURSER, J., AND MESINGER, F. A global-shallow water model using an expanded spherical cube. *Quart. J. Roy. Met. Soc.* 122 (1996), 959–982.
- [23] RITCHIE, H. Application of the semi-Lagrangian method to a spectral model of the shallow-water equations. *Mon. Wea. Rev.* 116 (1988), 1587–1598.
- [24] ROBERT, A. J. A stable numerical integration scheme for the primitive meteorological equations. *Atmos. Ocean* 19 (1981), 35–46.
- [25] RONCHI, C., IANOCO, R., AND PAOLUCCI, P. S. The ”cubed-sphere”: a new method for the solution of partial differential equations in spherical geometry. *J. Comput. Phys.* 124 (1996), 93–114.
- [26] SADOURNY, R. Conservative finite-difference approximations of the primitive equations on quasi-uniform spherical grids. *Mon. Wea. Rev.* 100 (1972), 136–144.
- [27] SHERWIN, S. A substepping Navier-Stokes splitting scheme for spectral/*hp* element discretisations. <http://www.ae.ic.ac.uk/staff/sherwin>, 2002.
- [28] STANFORTH, A., AND COTÉ, J. Semi-Lagrangian integration schemes for atmospheric models – A review. *Mon. Wea. Rev.* 119 (1991), 2206–2223.
- [29] STANFORTH, A., AND TEMPERTON, C. Semi-implicit semi-Lagrangian integration schemes for a barotropic finite-element regional model. *Mon. Wea. Rev.* 114 (1986), 2078–2090.

- [30] THOMAS, S. J., AND LOFT, R. D. Semi-implicit spectral element atmospheric model. *J. Sci. Comput.* *17* (2002), 339–350.
- [31] WILHELM, D., AND KLEISER, L. Stable and unstable formulation of the convection operator in spectral element simulations. *Appl. Numer. Math.* *33* (2000), 275–280.
- [32] WILLIAMSON, D. L., DRAKE, J. B., HACK, J. J., JAKOB, R., AND SWARZTRAUBER, P. N. A standard test set for numerical approximations to the shallow water equations in spherical geometry. *J. Comput. Phys.* *102* (1992), 211–224.
- [33] XIU, D., AND KARNIADAKIS, G. E. A semi-Lagrangian high-order method for Navier-Stokes equations. *J. Comput. Phys.* *172* (2001), 658–684.
- [34] XIU, D., SHERWIN, S. J., DONG, S., AND KARNIADAKIS, G. E. Strong and auxiliary forms of the semi-Lagrangian method for incompressible flows. *accepted for publication in J. Comput. Phys.* (2004).
- [35] XU, J., XIU, D., AND KARNIADAKIS, G. E. A semi-Lagrangian method for turbulence simulations using mixed spectral discretizations. *J. Sci. Comput.* *17* (2002), 585–597.

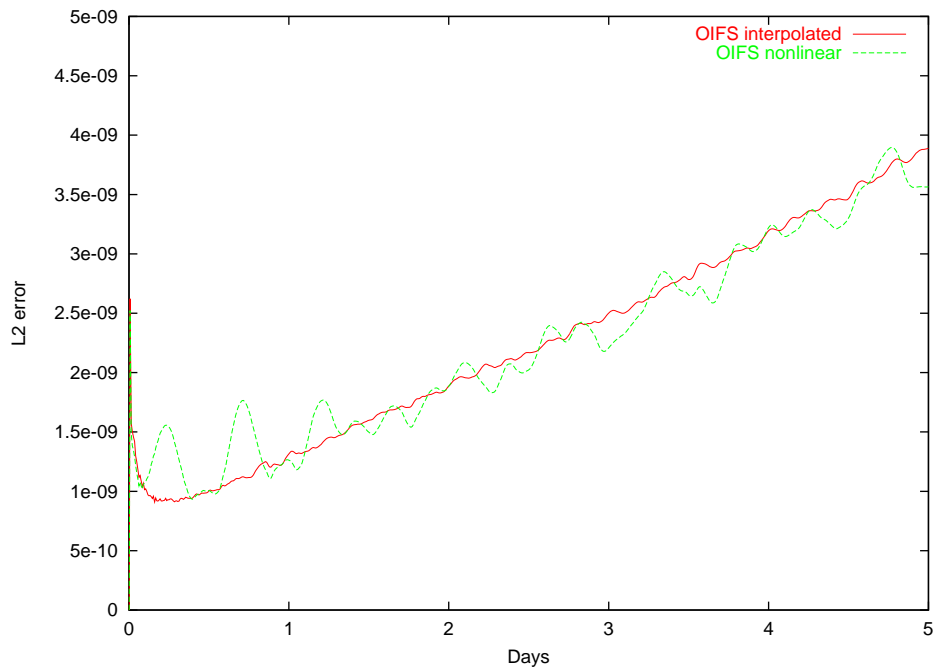


Fig. 1. Shallow water test case 2: Steady-state geostrophic flow. Geopotential height l_2 errors for extrapolated (solid red) and nonlinear (dashed green) OIFS schemes for a five day integration, $\Delta t = 120$ sec. Fischer-Mullen filter viscosity factor $\mu = 0.01$. $K = 96$ spectral elements, 14×14 Gauss-Legendre points per element.

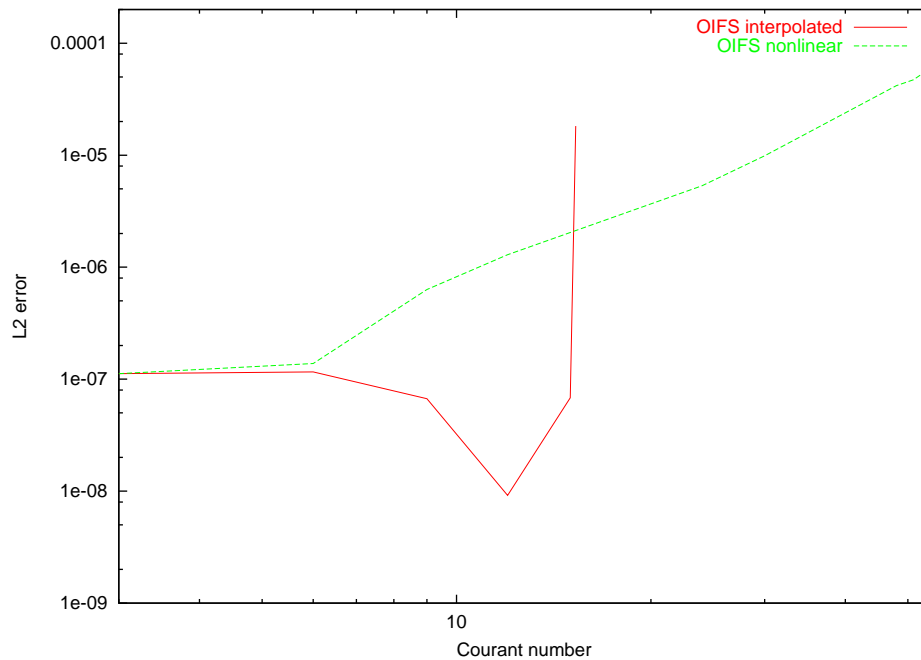


Fig. 2. Shallow water test case 2: Steady-state geostrophic flow. Geopotential height l_2 errors for extrapolated (solid red) and nonlinear (dashed green) OIFS schemes versus time step (scaled by the explicit CFL) for a five day integration Fischer-Mullen filter viscosity factor $\mu = 0.001$. $K = 150$ spectral elements, 8×8 Gauss-Legendre points per element.

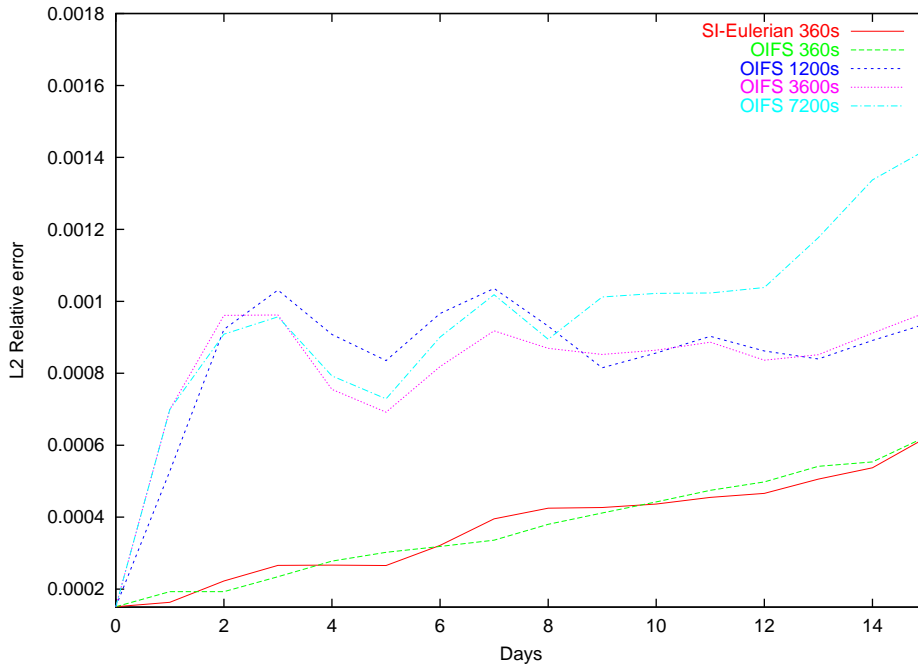


Fig. 3. Shallow water test case 5: Flow impinging on a mountain. Geopotential height l_2 errors for a 15 day integration using the the nonlinear OIFS scheme. Crank-Nicholson/leap-frog (CNLF) semi-implicit and BDF-2/RK-4 schemes are compared for various time steps. Fischer-Mullen filter viscosity factor $\mu = 0.01$. $K = 150$ spectral elements, 8×8 Gauss-Legendre points per element.

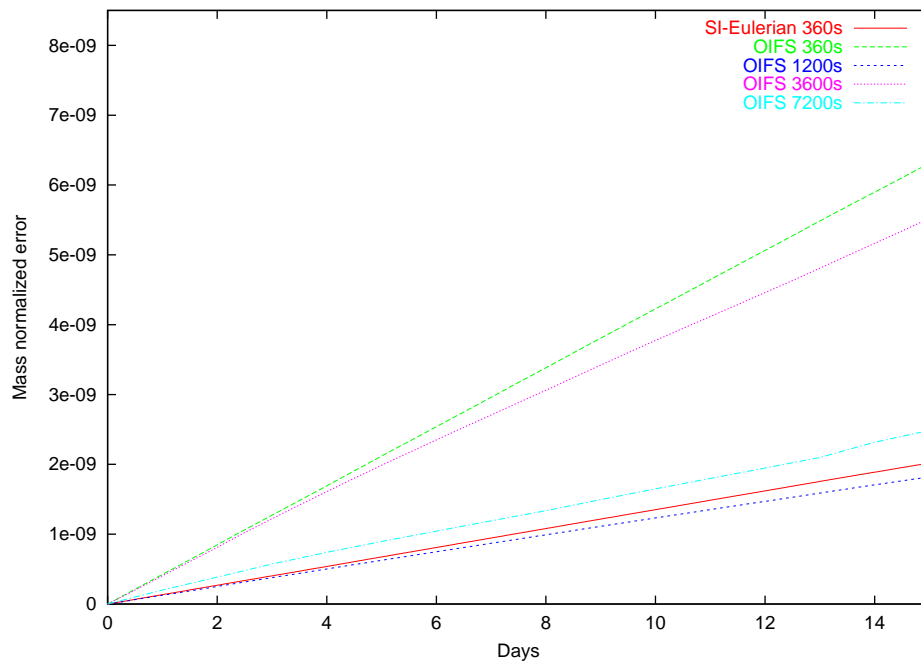


Fig. 4. Shallow water test case 5: Flow impinging on a mountain. Relative mass loss for a 15 day integration. Comparison of Crank-Nicholson/leap-frog (CNLF) and BDF-2/RK-4 schemes. Fischer-Mullen filter viscosity factor $\mu = 0.01$. $K = 150$ spectral elements, 8×8 Gauss-Legendre points per element.

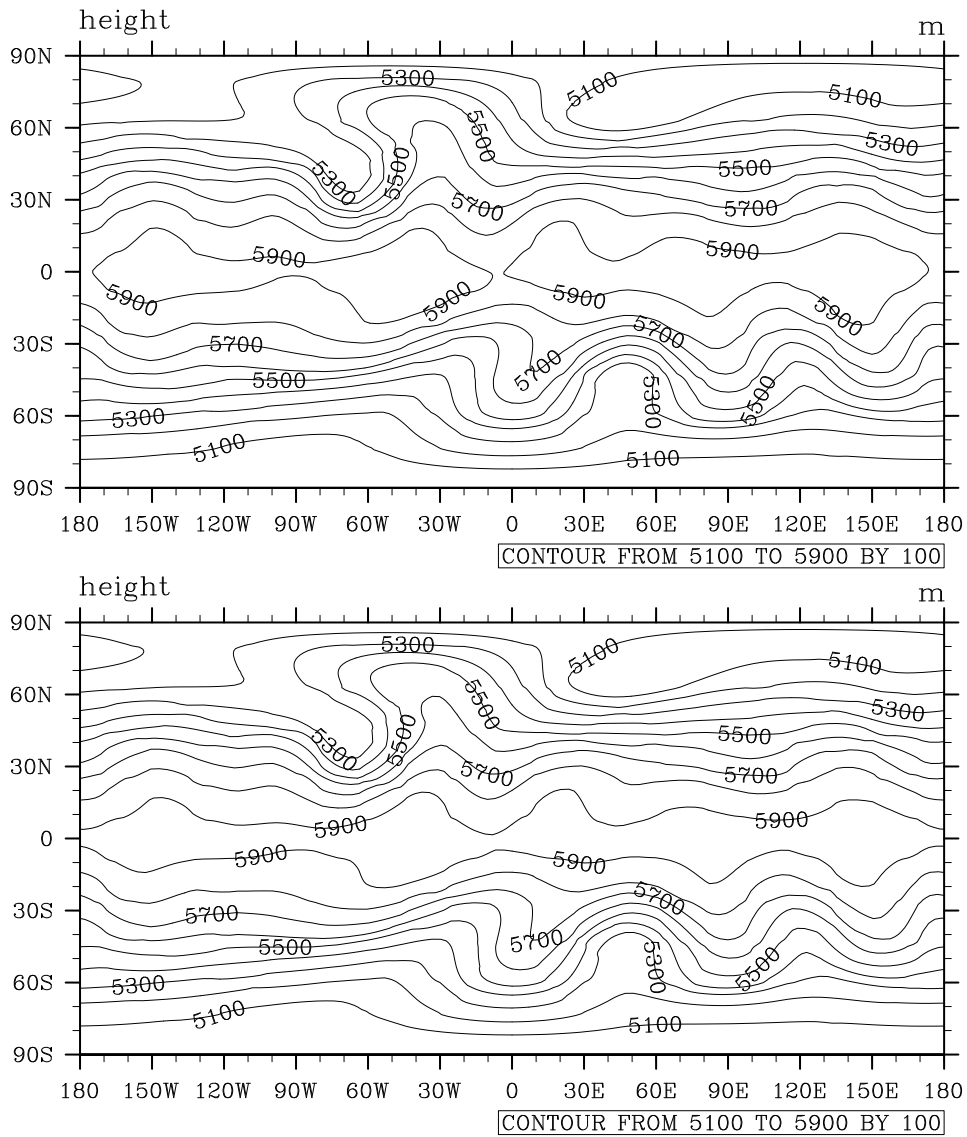


Fig. 5. Shallow water test case 5: Flow impinging on a mountain. Geopotential height field h at fifteen days produced by BDF-2/RK-4 scheme. Time steps $\Delta t = 480$ sec (top panel) and $\Delta t = 7200$ sec (bottom panel). Fischer-Mullen filter viscosity factor $\mu = 0.01$. $K = 150$ spectral elements, 8×8 Gauss-Legendre points per element.

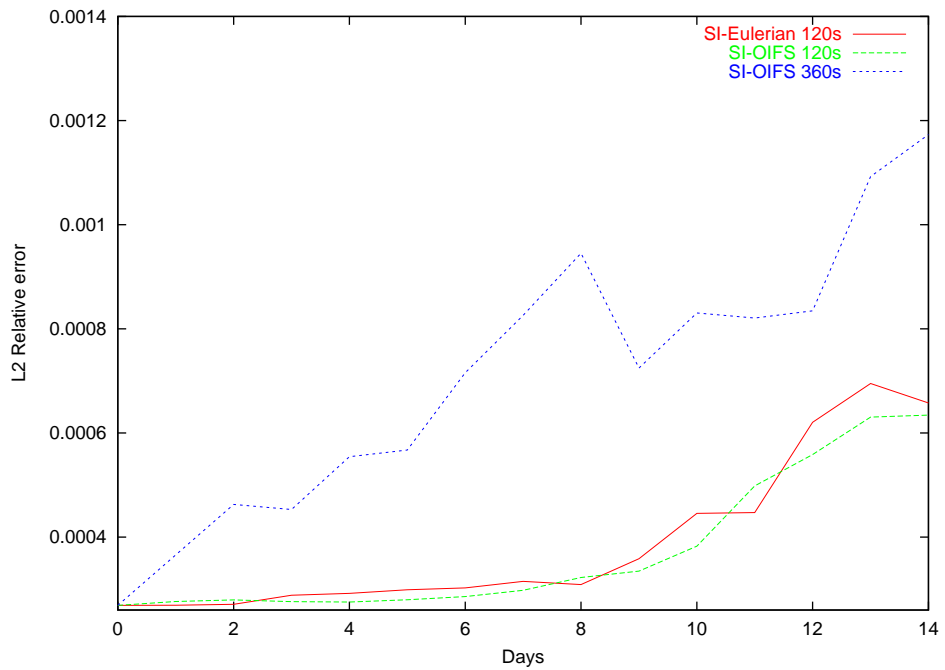


Fig. 6. Shallow-water test case 6: Rossby-Haurwitz wave. Geopotential height l_2 errors for a 14 day integration. Comparison of CNLF and BDF-2/RK-4 integration schemes. Fischer-Mullen filter viscosity factor $\mu = 0.01$. $K = 1734$ spectral elements, 8×8 Gauss-Legendre points per element.

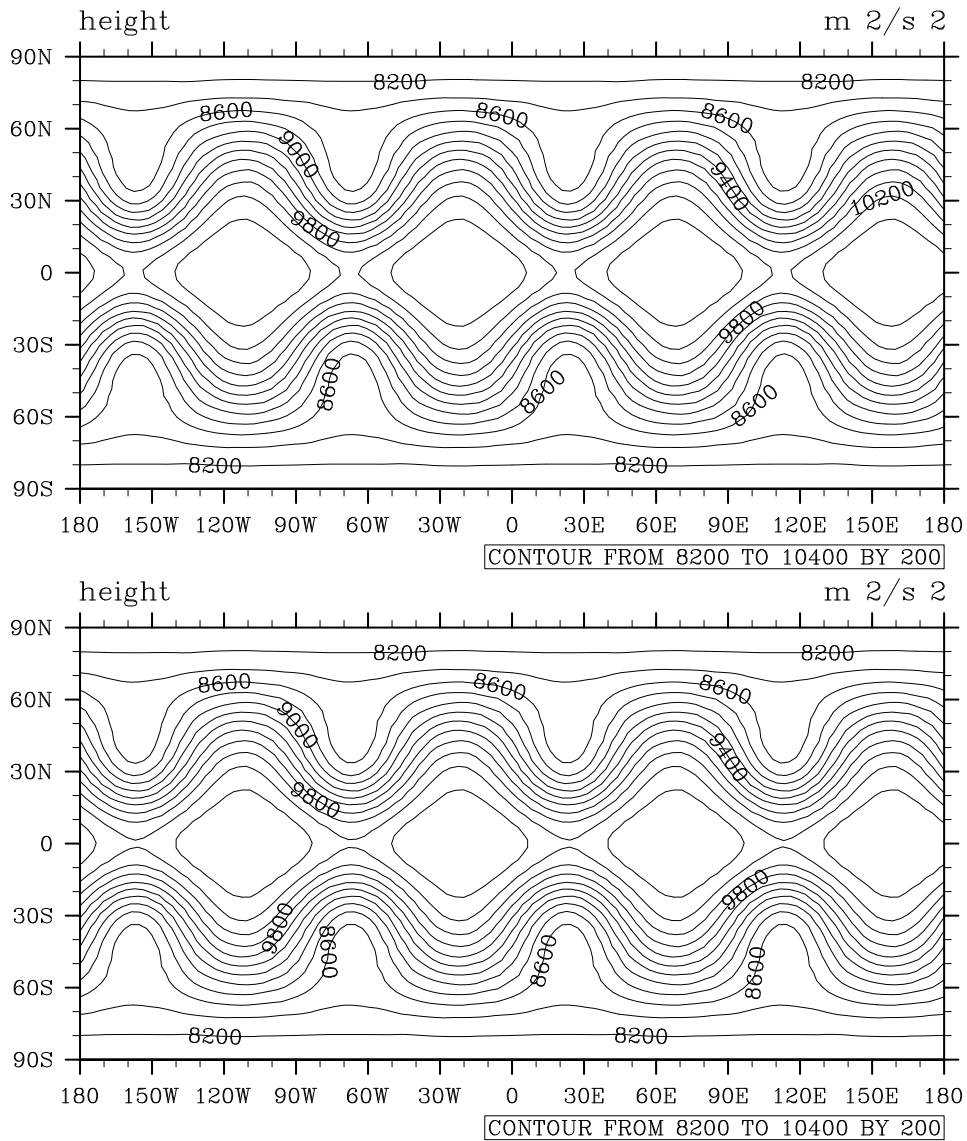


Fig. 7. Shallow-water test case 6: Rossby-Haurwitz wave. Geopotential height field after 14 day integration. Top panel: $\Delta t = 120$ sec. Bottom panel: $\Delta t = 360$ sec. $K = 1734$ spectral elements, 8×8 Gauss-Legendre points per element.

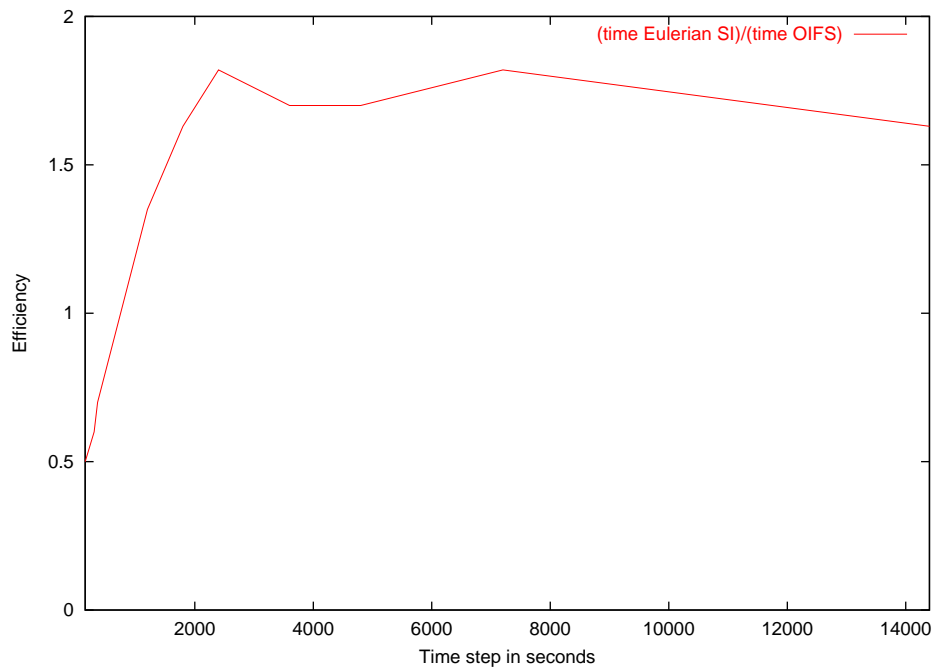


Fig. 8. Shallow water test case 5: Flow impinging on a mountain. Computational efficiency. Ratio of the CNLF and BDF-2/RK-4 model execution times. Fischer-Mullen filter viscosity factor $\mu = 0.01$. $K = 150$ spectral elements, 8×8 Gauss-Legendre points per element.